Iowa Initiative for Artificial Intelligence

Final Report

Project title:	Rapid Diagnosis of Aortic Valve Insufficiency in Aortic Root Enlargement
Principal Investigator:	Arun Singhal, Rodrigo Bello, Sarah Vigmostad
Prepared by (IIAI):	Honghai Zhang, Zhi Chen
Other investigators:	
Date:	04/01/2026

Were specific aims fulfilled:	Y
Readiness for extramural proposal?	In part -additional results needed
If yes … Planned submission date	
Funding agency	
Grant mechanism	
If no … Why not? What went wrong?	Further preliminary investigation is needed because the results of this project indicate: 1) potential different disease progression models, and 2) insufficient data for aortic dissection patients.

Brief summary of accomplished results

- The customized semi-automated segmentation workflow has proven to be efficient and applicable to images with varying quality. Hundreds of 3D images were analyzed.
- Using ML-based prediction methods, the results demonstrated that ascending aorta aneurysm is associated with various geometric features beyond increased diameter.
- Unfortunately, the prediction of progression (changes in maximal diameter) of aneurysm failed due to lack of longitudinal data with substantial changes.
- The results also showed potential in identifying aneurysm patients with higher risk of aortic dissection.
- Several limitations of the experimental design were identified, and directions for further preliminary studies using a different disease trajectory model were identified.

Research report

Aims (provided by PI)

Because clinical transthoracic echocardiography data is limited to 2D images without spatial information that specifies the 3D location of the 2D slice, echo data is not used in this project. Due to data availability, the study population is changed to patients with ascending aorta aneurysm (AAA) instead of aortic valve insufficiency and aortic root aneurysm. The modified aims are as follows.

1. Construct a customized workflow to perform semi-automated segmentation of the ascending aorta and three sinuses of the aortic root and compute a comprehensive set of geometric features.
2. Assess whether AAA is associated with geometric features beyond increased maximal diameter.
3. Assess the possibility of predicting AAA progression using ML methods trained on longitudinal data.
4. Assess the possibility of predicting AAA associated risk of aortic dissection.

Data

- Aim 2: 218 CT scans of 218 aneurysm patients.
- Aim 3: 494 longitudinal CT scans of 134 aneurysm patients, each with at least 3 CT scans.
- Aim 4:
  - 111 pre-surgery CT scans of aneurysm patients who underwent AA repairment surgery.
  - 11 pre-dissection CT scans of 11 AA dissection patients.
  - 82 CT scans of 82 normal patients selected from AortaSeg24 and AVT public datasets.

AI/ML Approach

Each CT scan is assigned to a label representing the stage or status of aneurysm. The ML model was trained using random forest or XGBoost classifier to predict AA stage or status.

For Aims 2 and 3, the maximal diameter (as continuous value) was also predicted with a regression ML model.

5-fold cross validation was used for all ML models.

Experimental methods, validation approach

<u>Aim 1: Semi-automated segmentation</u>

The LOGISMOS segmentation of ascending aorta uses a tubular mesh surface and is illustrated in Figure 1 with the following steps.

1. Approximate centerline of the ascending aorta from manually defined a start point at the sinotubular junction (STJ), an end point before brachiocephalic artery, and an optional point in between. Construct the initial mesh using evenly distributed vertices on cross-sectional slices that are perpendicular to the centerline.
2. Extend centerline into left ventricular outflow tract (LVOT) region such that all cross-sectional slices in the extended region are parallel to the STJ cross section. Create cylindrical visualization and perform automated LOGISMOS segmentation.
3. Adjust the centerline either automatically by computing centers of cross-sectional slices or manually by modifying locations of control points of the spline associated with the centerline.
4. Repeat steps 2-3 if necessary.

The LOGISMOS segmentation of aortic root sinuses uses spherical mesh surfaces and is illustrated in Figure 2. The three objects to be segmented are left, right, and non-coronary sinuses referred to as LCS, RCS, and NCS, respectively. Spheres are manually placed on the 3D image for cylindrical visualization to enclose the sinuses and initialize LOGISMOS segmentation. Figure 3 shows the resulting segmentations of all four structures from a normal subject and a patient with aneurysm.

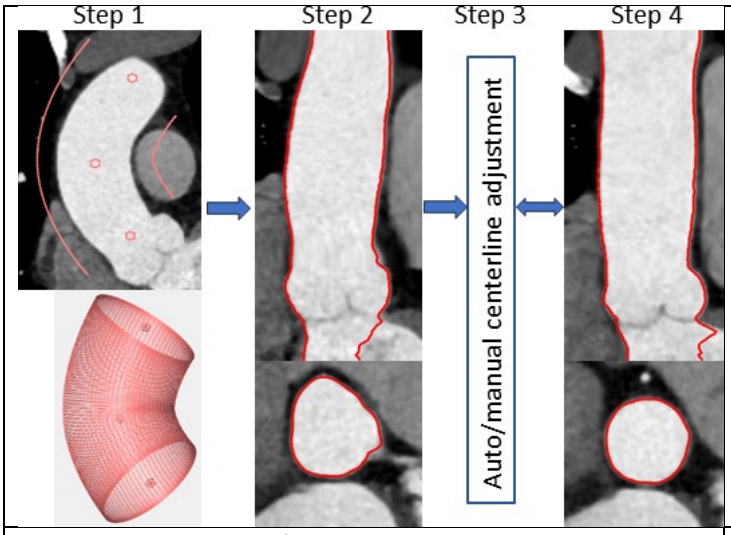

Figure 1. Illustration of semi-automated ascending aorta segmentation workflow.

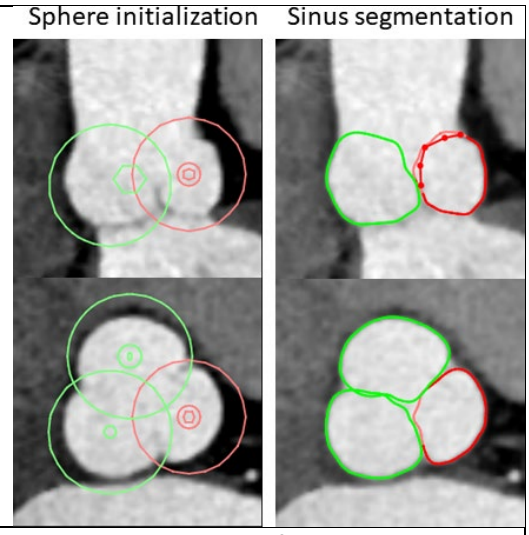

Figure 2. Illustration of semi-automated aortic root sinuses segmentation workflow.

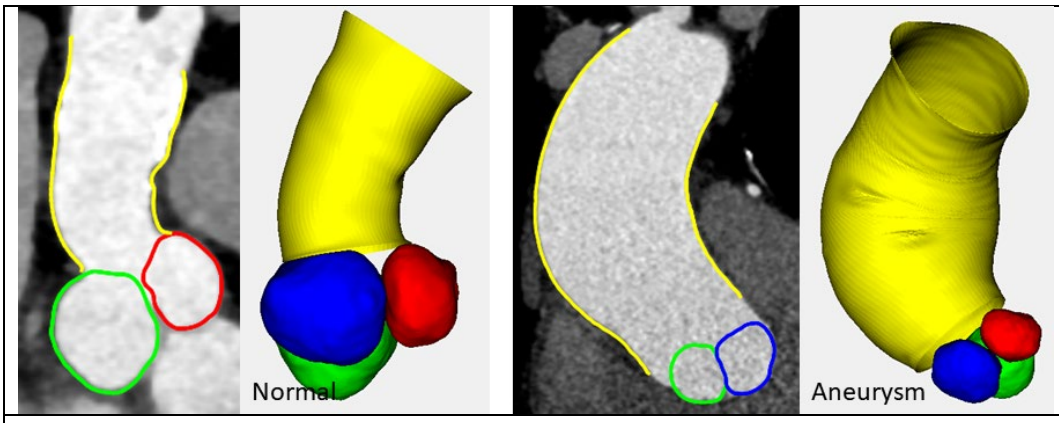

Figure 3. Examples of final ascending aorta and aortic root segmentation results. Red: LCS. Green: NCS. Blue: RCS. Yellow: ascending aorta.

Aim 1: Geometric Features

For ascending aorta, the following geometric features were computed from the segmentation results and illustrated in Figure 4.

- 14 3D shape features computed by PyRadiomics using default parameters after resampling with 0.5mm^3 voxels.
- Centerline length: length of 3D AA centerline (blue contour in Figure 4).
- Centerline cord length: length between the start and end points of centerline (line AC in Figure 4).
- Maximal centerline-to-cord distance: maximal distance between a point on centerline and the above cord (BD, perpendicular to AC, in Figure 4).
- Angle ∠ABC in Figure 4.
- Relative position of point B in Figure 4 as length of contour BC divided by centerline length.

- Centerline curvatures measured at 0% (STJ), 5%, …, 95%, 100% centerline length locations.
- Cross sectional shape eccentricities measured at 5n% centerline length locations.
- Cross sectional diameters measured at 5n% centerline length locations.

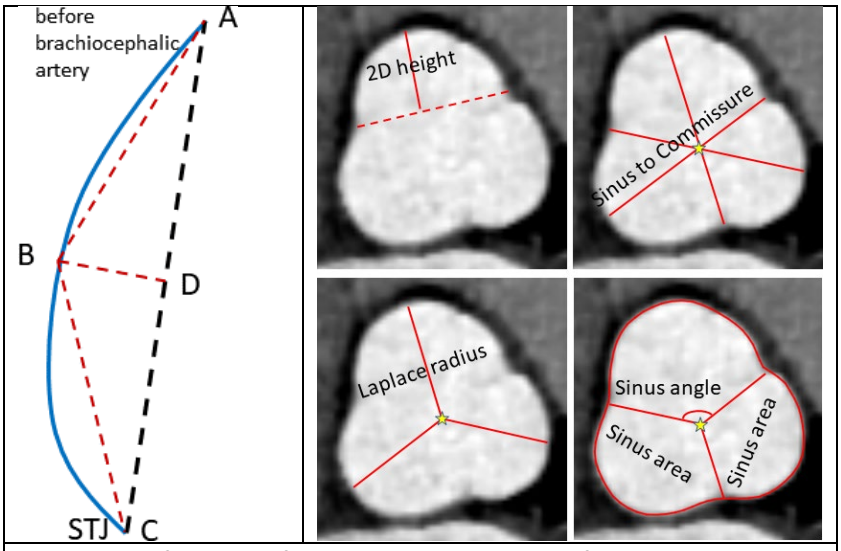

Figure 4. Definitions of centerline and 2D sinus features.

For each AoR sinus, 14 3D shape features were computed by PyRadiomics using default parameters after resampling with 0.5mm^3 voxels. These features include volume, surface area, surface area to volume ratio, sphericity, elongation, flatness, etc.

For AoR sinuses, an additional set of 2D features were computed at sinus of Valsalva (SoV) as shown in Figure 4. The SoV cross-sectional slice was chosen on the cylindrical view (Figure 8) as the first cross-sectional slice below (distal to) the left and right coronary arteries on which all three commissures can be identified. These 2D features include sinus height, sinus-to-commissure distance, sinus-to-sinus distance, Laplace radius, sinus angle, sinus area, etc.

Because LOGISMOS uses tubular mesh (Figure 1) as the inherent data representation for the ascending aorta, constructing statistical shape model (SSM) for the ascending aorta becomes more straightforward. In this study, two independent shape models were constructed for the centerline and cross sections (radius map) of the ascending aorta.

Each ascending aorta centerline associated with the segmentation was resampled to have 51 uniformly distributed (evenly spaced with 5% total length in-between) points. The Iterative Closest Point (ICP) algorithm was used to align all centerlines. Principal Component Analysis (PCA) was applied to all aligned centerlines. For Aim 2 data, the 3 most significant PCA modes cover 95% of total variation. The variations associated with these PCA modes are shown in Figure 5.

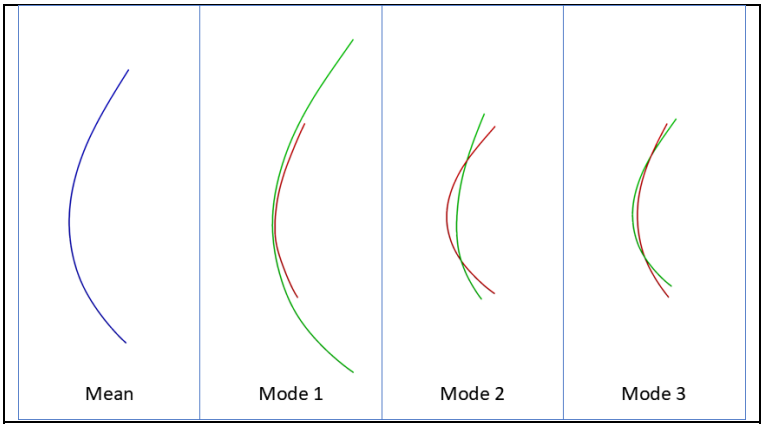

Figure 5. Mean shpe of ascending aorta centerline and variations associated with 3 most significant PCA modes.

As shown in Figure 6, each cross-sectional slice of the tubular mesh of the segmented AA surface has 72 vertices with a 5-degree angle increment in-between with respect to the corresponding centerline point. The tubular mesh can be unwrapped (cut open) to form a 2D radius map whose pixel value represents the local radius -- the distance between mesh vertex and corresponding centerline point. Generating a 51-slice radius map can be achieved by either creating a 51-slice mesh via centerline resampling first or linear interpolation of x-slice radius map utilizing the known x-point centerline. The reference contour (purple in Figure 6) for unwrapping was chosen based on the aortic root commissure between LCS and RCS that is manually identified (Figure 8). For Aim 2 data, the 3 most significant PCA modes cover 95% of total variation. The variations associated with these PCA modes are shown in Figure 7.

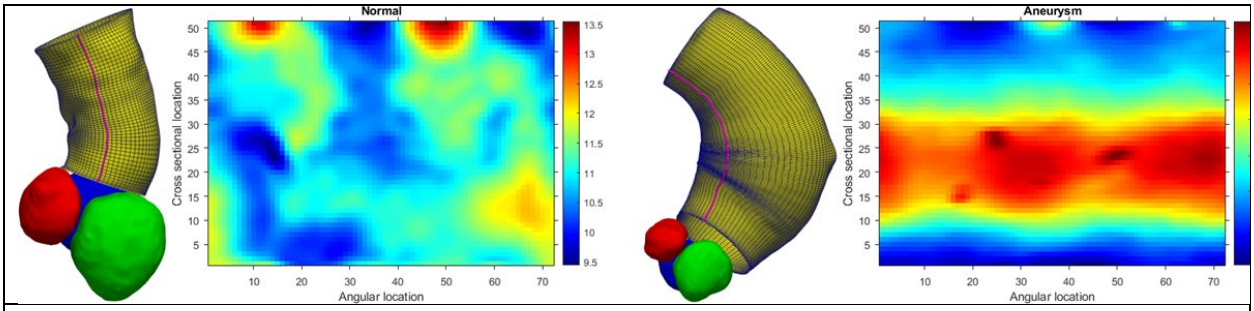

Figure 6. Creating ascending aorta radius maps. Purple contour is the reference contour for which the tubular surface is unwrapped into a radius map.

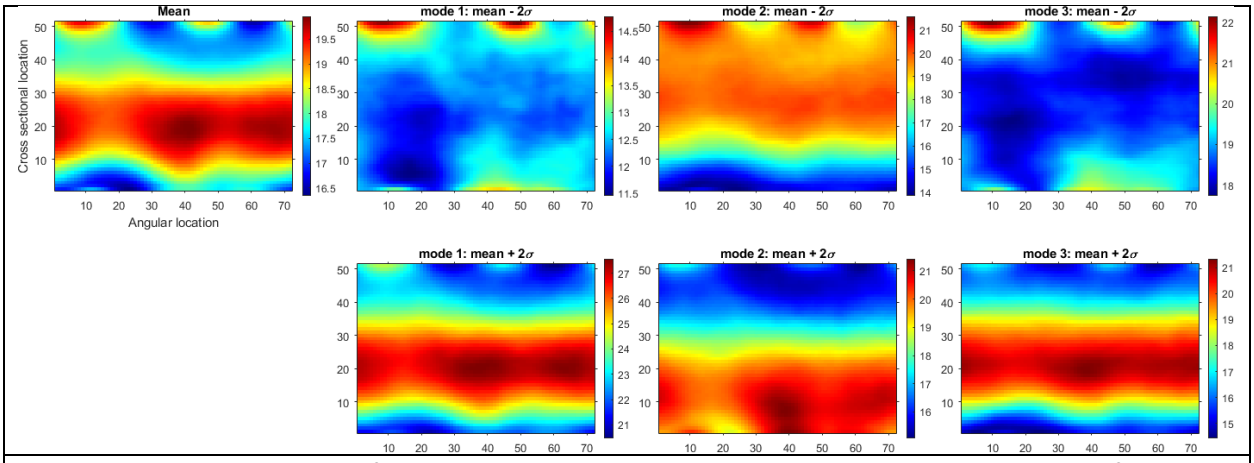

Figure 7. Mean radius map of ascending aorta and variations associated with 3 most significant PCA modes.

Aim 2: Predicting aneurysm stages

Based on the maximal diameter of the ascending aorta, four stages of aneurysm were assigned to all 218 patients. Random forest model was trained to predict AA stage and regression model was trained to predict maximal diameter values. All features that are directly related to the AA maximal diameter, such as cross-sectional diameters measured at 5n% centerline length locations, were excluded from the inputs to the model.

For predictions on labeled stages, confusion matrix and traditional metrics derived from it were used to evaluate the performance of the prediction. For continuous diameter prediction, the predicted values were compared with the truth values using linear regression.

Aim 3: Predicting aneurysm progression

The first available CT scan of a patient was used as the baseline scan T0. The maximal AA diameters of all follow-up scans were used together with the time intervals between longitudinal scans to compute (via linear interpolation) maximal diameters at T1yr and T2ry (one year and two years after T0).

The regression model was trained to use all features at T0 to predict the maximal diameter at T1yr and use all features at T0 and T1yr to predict T2yr. The performance of prediction was evaluated by comparing predicted and true values using linear regression.

Aim 4: Predicting dissection risk

Three risk labels were assigned to the study population. Scans from AortaSeg24 and AVT public datasets were labeled as *normal*. The scans of UIHC patients without surgery were labeled as *low risk*. The pre-surgery and pre-dissection scans were labeled as *high risk*.

Two XGBoost models were trained, one for distinguishing low-risk and high-risk scans, the other for distinguishing all scans of the three risk groups. The performance was evaluated with the confusion matrix and its derived metrics.

Results

Aim 1: Semi-automated segmentation and feature extraction

The semi-automated segmentation workflow that is illustrated in Figures 1-3 turned out to be very efficient. The total time spent analyzing one CT scan by the human operator was between 5-10 minutes. High-quality CT scans (ECG-gated, high-resolution, low noise and artifacts) often only require approximately 5 minutes. Additional efforts in locating landmarks (e.g. STJ) and reasonable depiction of sinus surface were required on low-quality CT scans. After occasional localized segmentation error correction via JEI, all segmentations were deemed satisfactory by visual inspection.

Aim 2: Predicting aneurysm stages

The definition of aneurysm stages based on maximal diameter and the resulting random forest prediction were shown in the following Table 1, where the accuracy of absolute correct prediction is 64.2%. If we consider the 'one-off' predictions (green numbers) acceptable, the corresponding adjusted accuracy is 90.7%. The top 3 features that contribute most to the prediction are: AA centerline length, AA centerline cord length, and AA maximal centerline-to-cord distance.

Table 1. Result of aneurysm stage prediction.

True \ Predicted	<40 mm	40-45 mm	45-50 mm	>50 mm	Row total
<40 mm	98	9	3	0	110
40-45 mm	17	25	10	0	52
45-50 mm	8	11	14	2	35
>50 mm	3	4	10	1	18
Column total	126	49	37	3	215

The results of predicting maximal diameter using a regression model are shown in Figure 8. Note that in this case the diameters (local and global maximal) are not part of the model input, and the predicted maximal diameters are highly corelated to the true values.

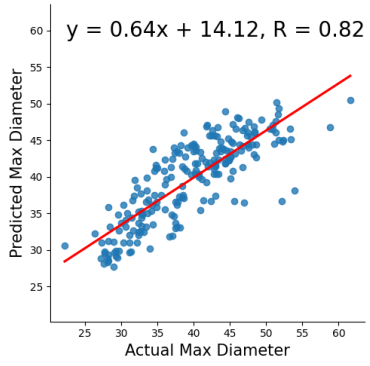

Figure 8. Linear regression of diameter prediction.

Aim 3: Predicting aneurysm progression

The results of aneurysm progression (changes in maximal diameter over time) prediction are shown in Figure 9. At first glance, Figure 9a and 9c show that the model produces very good predictions on maximal diameter one year after the latest scan. However, feature important analysis (Figure 9b and 9d)

shows that the role of the maximal diameter at T0 substantially exceeds that of the other features, which are also closely related to maximal diameter. Such results suggest that the dataset does not contain enough samples with apparent longitudinal changes of maximal diameter and therefore a simple prediction of 'no change' is a very good prediction.

The longitudinally static nature of the available data is verified by plotting longitudinal changes in diameter as well as in centerline length of each patient. Due to this limitation of the data, we have to admit failure on Aim 3.

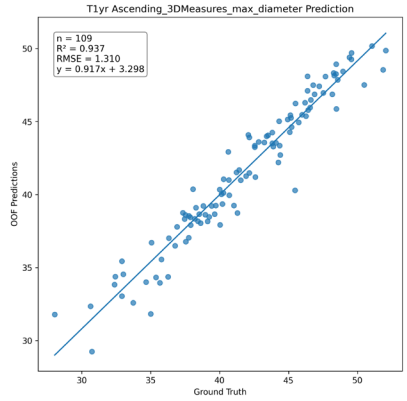

a) T1yr truths vs. predictions.

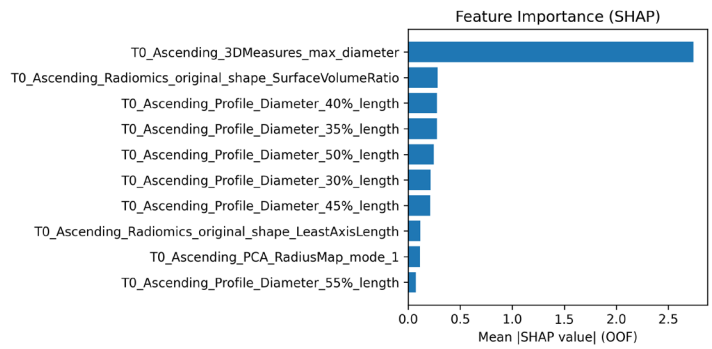

b) Feature importance of T1yr predition.

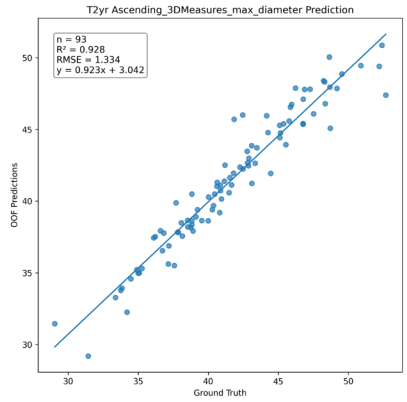

c) T2yr truths vs. predictions.

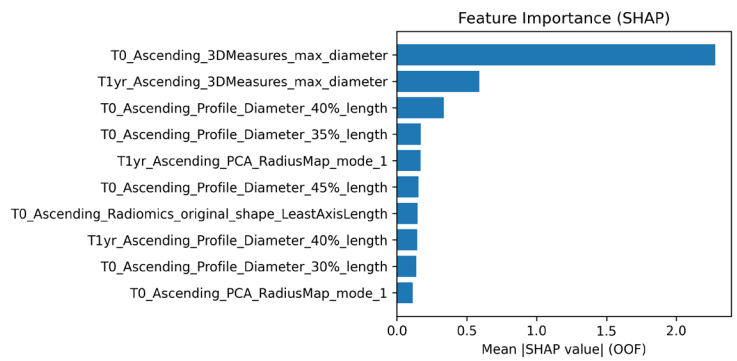

d) Feature importance of T2yr predition.

Figure 9. Results of aneurysm progression prediction.

Aim 4: Predicting dissection risk

Table 2 lists the performance of two-class risk predictions with and without using demographic features that are age, sex, race, weight and height. Table 3 lists the results of three-class prediction without using demographic features. The numbers of low- and high-risk patients in these tables are slightly different because the experiments were conducted at different times.

Table 2. Results of two-class risk prediction.					
Demographic & geometric features			Geometric features only		
True \ Predicted	Low risk	High risk	True \ Predicted	Low risk	High risk
Low risk	90	35	Low risk	76	45
High risk	41	78	High risk	34	87

Table 3. Results of three-class risk prediction.			
True \ Predicted	Normal	Low risk	High risk
Normal	76	3	3
Low risk	6	98	30
High risk	3	38	80

Ideas/aims for future extramural project

Aorta segmentation and feature extraction

One of our earlier hypotheses is that the progression of aneurysm is associated with the changing of asymmetry of aortic root sinuses that can be described by one or several intuitive measures. Therefore, the three sinuses were individually segmented and measured by a comprehensive set of 2D and 3D geometric features. During the fulfilment of Aim 1, several limitations of such sinus-oriented features were identified.

For any given sinus, only approximately half of its 3D surface – the part on the outer wall and the aortic valves (if sufficiently depicted) – can be segmented based on reliable image information. The other half of the 3D surface is mainly estimated based on 3D context with respect to the other two sinuses and smoothness constraints. Such uncertainties can substantially affect the reliability of any volume-based features. In other words, clearly visible aortic outer wall and valve surfaces *does not* mean that the aortic root volume can be reliably divided into three sinuses.

By looking at Figure 4 alone, the 2D sinus features appear to have simple definitions and are easy to measure. However, finding such an oblique plane with three clearly depicted clovers is time consuming, subject to observer variability, and only feasible on high-quality CT scans. Furthermore, these 2D measures oversimplify the potentially more complex 3D shapes of root or sinuses.

The feature importance analysis of all prediction models showed that the top 20 most important features are mostly features of the ascending aorta, and there is no sinus feature that is consistently important for all models. It suggests that a single (or several) sinus asymmetry feature that is easy to understand, easy to measure, and highly related to aneurysm probably does not exist. In the future, segmenting the whole aortic root as a single object and computing 3D geometric features will be more reliable and efficient. Additional experiments (results not included) showed that segmenting whole root requires much less user interaction and error correction and can be potentially fully automated using AI methods once enough high-quality training data is collected by using the current semi-automated approach.

The length and shape of the ascending aorta are often among the top important features of our prediction models, suggesting that they are the most important secondary (other than increasing

diameter) aneurysm features. Although it is known that the embryological origin of the ascending aorta is different from that of the aortic arch and the descending aorta, analyzing all these sections of the aorta may provide more insight into AA aneurysm. Additional experiments (results not included) showed that extending the current workflow to segmentation and analysis of all three aortic sections is feasible with only slightly more user involvement and can be potentially fully automated using AI methods once enough high-quality training data is collected by using the current semi-automated approach.

Using extracted features to understand aneurysm characteristics, progression and associated risk

Various experiments were constructed for Aims 2-4 to test the capability of using derived features to advance our knowledge of aneurysm characteristics, progression, and associated risks. The results suggest that the main limitation of achieving so is the availability of data.

The UIHC data used in Aim 2 were collected in two separate batches (XNAT projects), one targeted for normal data, and the other for aneurysm data. However, some of the scans in the normal batch have clearly visible aneurysms. Instead of labeling all scans in the normal batch as normal, the scans from both batches that produced acceptable segmentation were used in Aim 2 and the stages were derived from the maximal diameter measured. Note that this dataset is slightly unbalanced with only 8% >50 mm diameter.

Despite the large number of patients and scans collected for the longitudinal study for Aim 3, no rapid grow was observed in the data, which leads to the failure of Aim 3. In the future, we should pay extra attention to mining the clinical record to identify patients with various growth to be included in longitudinal studies.

The normal dataset used in Aim 4 comes from public datasets, for which no clinical details of the patients are available. The reasons that dataset was used are: 1) they have lower quality than our own UIHC data and allowed us to test the robustness of Aim 1 method; 2) they appear to be free of aortic abnormality and allow us not to wait for actual verified normal data from UIHC. In the future, we should dedicate efforts to collect verified normal data.

The pre-surgery scans in Aim 4 are labeled as high risk. But in real-world circumstances, the decision of surgery is not made only based on diameter; other physical and mental quality-of-life factors are also considered. It is possible for a high-risk scan to contain no high-risk geometric features such as a substantial increase in diameter or length.

Although the results of Aim 4 indicate that aneurysm and dissection may follow different trajectory – increased diameter does not necessarily lead to dissection and dissection can happen without obvious aneurysm. Collecting enough pre-dissection data is extremely difficult.

The current approach of identifying patient data to be studied is to use a small number of fields (entries) of the clinical record to locate patients and collect all CT data. This leads to additional efforts to visually check and identify those that meet the requirements and can be analyzed.

- More than 3600 scans of more than 1100 patients were collected for Aim 3.
    - The 494 scans of 134 patients were found to meet the more-than-3-scan and good-quality criteria after checking half of the 3600 scans. Other than less than 3 scans, the main cause of exclusion was insufficient quality due to non-gated acquisition.

    - The 111 pre-surgery scans in Aim 4 were also identified from this dataset after every scan was visually checked.
- 190 scans of 140 patients were collected for the dissection population in Aim 4.
    - Only 11 pre-dissection scans were found, and they are of lower quality than those for Aim 3.

For future projects, especially those for R01 applications, the estimation of available study population size should be made with extreme cautious. Considering the lessons learned above, the number of patients with certain conditions that are seen in the clinic and scanned with CT could be very misleading.

Table 4 lists the CT data used by other reported pre-dissection related studies. It shows that less than **5%** of the patients have CT scans within 2 years before the onset of dissection. Note that certain target geometric features can only be derived from high quality CT and can further reduce the number of analyzable scans. For example, the study in 10.1016/j.atssr.2025.06.032 measured aortic root features on an oblique plane where all three sinuses are clearly depicted with a clover-like shape. Such image quality requirement made 18 originally identified pre-dissection scans unusable. Such rarity of pre-dissection scans may lead to further issues as follows.

- A study population that includes aneurysm and dissection patients will always be heavily unbalanced for statistical comparison of aneurysm and dissection as well as machine learning methods for classifying or predicting dissection.
- It is not clear whether characteristics seen on pre-dissection CT represent the whole dissection population.

Table 4. Data summary of reported pre-dissection CTA studies

DOI	Country	Time span (years)	# of dissection patients	# of analyzed pre-dissection CT
10.1016/j.atssr.2025.06.032	USA		212	14
10.1016/j.compbiomed.2024.109310	USA			8
10.1093/ejcts/ezw025	Germany	9	146	16
10.1016/j.jacc.2013.12.028	US + Europe, 6 centers	9	1821	63
10.1136/heartjnl-2019-316251	Netherlands, 2 centers	9	477	25
10.1093/ejcts/ezaf053	Italy, 2 centers	5		15
Total			**>2656**	**141**